On estimating the Location and the 3-D shape of an Object in an Indoor Environment Using Visible Light

Aranya Chakraborty*, Anand Singh+, Vivek Ashok Bohara+, and Anand Srivastava+
*Indian Institute of Science, Bengaluru, India, 560012
+Wirocomm Research Group,
Department of Electronics & Communication Engineering
+IIIT-Delhi, New Delhi, India, 110020

Abstract- The recent interest in using visible light as a means of communication has opened up possibilities for using visible light for other applications as well, such as indoor positioning. Visible light offers higher bandwidth, immunity from electromagnetic radiation, and most importantly it can be seamlessly integrated into the existing lighting infrastructure. This paper proposes a visible light based positioning model for estimating an object's three-dimensional (3-D) parameters such as height and radius in addition to location in an indoor environment. The model is built using neural networks (NN), trained by simulating numerous multiple object scenarios in an indoor environment. It also takes into account the shadowing effects so it can be implemented in a multiple obstacle environment. The proposed algorithm has numerous applications, such as positioning assisted communication, suspicious object monitoring and surveillance in an indoor environment. The proposed model achieves a location accuracy of 5.4 cm, which could be further improved to 4 cm at the expense of extra hardware. The accuracy in measuring the height and radius of the objects using the proposed framework is observed to be 4.39 cm and 1.27 cm, respectively. In addition, we also propose a methodology to optimize the power distribution to the light-emitting-diodes (LED's) in order to get the optimum location accuracy while maintaining the total power constraint on the system. This method could be utilized to update the power allocated to the LEDs by exploiting the current location of the objects in the room to improve communication uplink by employing visible access points (VAP's).

***Index Terms*—Visible Light Communication (VLC), Indoor positioning, Matern hard core point process (MHCP), Light-emitting-diodes (LEDs), Artificial Neural Network (ANN).**

I. INTRODUCTION

Indoor positioning has gained considerable traction recently due to its utility in different environments such as underground parking, office and home spaces, etc. Recently, a substantial amount of research has been devoted to developing more accurate models for indoor positioning, which could be attributed to the advancements in wireless sensor network technologies. Several indoor positioning technologies, such as pseudo-satellite (Pseudo lite), assisted global positioning systems like (A-GPS), Zigbee, Bluetooth (BT), wireless local area network (WLAN), ultra-wideband radio (UWB), radiofrequency tags (RFID), infrared, computer vision, magnetic, ultrasonic and visible light are being considered to achieve high-accuracy indoor positioning and navigation systems [1]–[4]. However, GPS positioning results in significant path loss due to attenuation by the room walls. Similarly, UWB-based positioning has very low signal strength, which makes it unsuitable for large indoor spaces. Further, WLAN-based positioning requires a complicated setup, and the accuracy is also quite low [5]. Other positioning methods, such as infrared, Zigbee, and Bluetooth, are vulnerable to fluctuations in signal sources [6]. Employing visible light for indoor positioning has recently become the subject of much investigation within academic and industrial research community [7]. Moreover, the LED-based visible light positioning (VLP) system also has great potential for practical applications such as light assisted communication, suspicious object monitoring, and surveillance in an indoor environment.

Visible light communication (VLC) has been widely used in indoor positioning, as evident from previous literature [7-14]. Its suitability for indoor positioning comes from the fact that it offers large bandwidth, high positioning accuracy, and immunity from electromagnetic interference. In addition, it requires no large-scale costs for deployment as it can be integrated seamlessly into the existing illumination setup.

VLC-based positioning techniques are of two types, photodiodes (PD) and image sensor (IS) based systems [8]. The usage of PD based system is more because they have high sensitivity to light, and they are less expensive, whereas IS can spatially separate light sources. But preference is given to IS based positioning technique because it does not need multiplexing techniques, and also, positioning exactness will not be influenced by surrounding light interference. The basic methodology is trilateration which uses visible light sources as anchors. In Epsilon [9], each bulb, with its lighting function, also serves as a site mark. It transmits, using the light carrier; location signals carries the information, which means the stance of the bulb and its duty cycle, to enable positioning on the end of the receiver part. An intelligent cell is used as a receiver that uses light sensors to extract the signal's information, and the received signal strengths (RSS) are measured [10] from many LEDs, and distance is calculated from each bulb using the optical channel model. Then, from all light sources, beacon information is received, and distances are measured, which helps to estimate the location. There are different methods for triangulation's like received signal strength indicator (RSSI), time of arrival (TOA), angle of arrival (AOA), and time difference of arrival (TDOA). There are different probing signals depending on the positioning system, like ultrasound, ultra-wideband (UWB), and wireless local area network (WLAN). As ceiling lights are visible from any place in an indoor environment, it works under line-

of-sight (LoS) conditions, which is why the received signal strength ratio (RSSR) is preferred [10]. Here the RSSR is the ratio of the received signal power (strength) at the PD to the transmitted signal power from the LED. In an indoor VLC system, RSSR is determined by the LED transmission power, the distance between the LED and the PD, and the respective VLC parameters such as LED irradiance angle, receiver field-of-view (FOV).

The two primary components required for visible light-based indoor positioning are the LED as transmitters and PD as optical receivers. There is a constant link between the LED and PD, which is only interrupted in the presence of an object blocking the LoS. Thus the changes in the channel characteristics in the presence of an object can be used to gather information about the object such as its position, shape etc. However, multipath propagation, shadowing and interference from various noise sources as well as form other objects in the vicinity affect the LED's transmitted optical signals [11]. Thus, finding suitable models for the VLP to achieve high positioning accuracy is a source of a considerable amount of research [12]. This paper builds upon the existing work on VLP and proposes a novel RSS based VLP system model for indoor positioning, which can be implemented by utilizing the existing lighting infrastructure. Specifically, the proposed VLP system model can be used to construct a 3-D rendering of a room with multiple objects. The objects in the room are modelled as cylinders[1] with varying heights and radius, leading to well-defined metrics for evaluating the performance of the algorithm [15]. Furthermore, this paper also presents a technique for allocating the power available to the LEDs in response to a particular arrangement of objects further increasing the accuracy of positioning.

A. Related Works

VLP has emerged as a tractable approach to localize objects in an indoor environment and various methods have been considered in recent literature for increasing the accuracy of VLP models. A simple regression-based approach for VLP with linear and nonlinear least square estimations (LLS & NLS) has been shown in [16]. It's performance is evaluated by various metrics such as the average localization error, standard deviation, and cumulative distribution function (CDF). One of the major contributions of [16] is employing the regression method to enhance the VLP system's performance. In [17], a novel positioning scheme is presented which utilizes both the received power profile as well as the angle of arrival (AoA) in order to increase positioning accuracy. An analytical expression for the Cramer-Rao lower bounds (CRLB) for RSS-based localization is also discussed, along with the effectiveness of the solutions under varying parameters. Further, techniques to increase the accuracy of VLP are proposed in [18] and [19]. In [18], a new responsivity model square (SQ) is proposed and in [19] an indoor positioning system that utilizes multiple PDs with a known calibration point is utilized to increase the accuracy of VLP. Both show an increase in VLP accuracy but at the expense of increased complexity. VLP accuracy can also be optimized by employing additional sensors in addition to a standard PD. In [20], Simon et al. have used a camera, an inclinometer, and a magnetometer sensor to determine the target's position. Similarly, in [21] authors combined the measurements from a camera, gyroscope, and encoder for positioning and the data is fused using multiple approaches, including an extended Kalman filter. In [22], Cheng et al. employed a CMOS camera and the geometric features of LED projection to improve the positioning accuracy. Although usage of multiple sensors increase the position accuracy it also leads to additional issues such as identifying a suitable algorithm to combine the measurements of different sensors. In [23], simultaneous positioning and orientating (SPAO) scheme was developed using a novel particle-assisted stochastic search algorithm, which provided a substantial technical improvement over the existing VLC localization solutions. Similarly, a visible light positioning system based on particle swarm optimization (PSO) algorithm is proposed in [24]. In [25], authors used many LEDs to form a low-complexity VLP model with sinusoidal waveforms. However the acquired signal suffered from a low signal-to-noise ratio, so the location estimation was repeated for overlapping received signal segments differing by a few samples. The mean of the resulting positions is taken to be the final estimate. In [26], a 3-D positioning scheme of a target terminal having multiple PDs is proposed. Using RSS measurements and the relative coordinates between the receiving PDs and fixed transmitting LEDs accurate positioning can be done by Los channels. Moreover, [26] also considered multipath reflections from the interior walls as non-line-of-sight (NLoS) channels, and it is observed that the positioning accuracy decreases linearly with the reflection coefficient of walls. The results are also verified by simulations.

It is noted that in the models presented in existing literature, a single PD is generally used to signify a user and the location of that PD is estimated by maximizing the likelihood of the received power profile matrix obtained from different transmitting LED's [17]. Consequently, most of the existing system models for VLP locate the objects as a point in 3-D space. In contrast, by utilizing the VLP system model proposed in this paper, the 3-D shape of the user can be identified. In addition, the proposed model facilitates passive modelling. Specifically, the target, which is being localized, need not possess a PD. For instance, passive objects, such as furniture in the room, can also be modeled by the proposed method.

In addition, the proposed model can also perform accurate positioning in the presence of multiple objects. Conventional VLP methods generally are inaccurate when multiple objects are present in a room since the objects may block the LoS path between the transmitter and other objects. As this model considers the objects as 3-D shapes, the effects of shadowing in the presence of multiple objects can be clearly observed and corrected. Moreover, in this paper, as stated before indoor positioning utilizes RSS based method. In order to obtain the RSS, we need to calculate the received power at the PD. Here, in this paper the received power is calculated based on the LED illumination power across the room in the

[1]In [13] [14], different geometric models representing the human body have been considered. It has been shown that the human body as a cylinder is the best-fit with respect to other models.

presence of human blockages. Hence for the received power profile calculation, LED need not be a communication source and may just function as a source of illumination Hence, the proposed VLP can facilitate improvement in positioning without significant changes to existing infrastructure. In this paper, we have considered 4 LEDs transmitting (broadcasting) the same data) at equal power. Since all the LEDs emit the same power, both RSSR and RSS methods are equivalent for a machine learning-based algorithm.

B. Contribution

The existing literature on VLP primarily focused on locating the object as a point in 3-D space. Although, this induces less operational overhead, it tends to overlook the information about the shape and size of the object. The estimation of the shape and size of the object is especially important when multiple objects are present in the room. In this work, which builds upon the work presented in [15], we overcome the above drawback by proposing a novel VLP model which estimates an object's 3-D parameters along with its location in an indoor environment. The major contributions of this paper are summarised as follows:

1) In this paper, we propose a novel system model for VLP, which can be used to estimate the location of objects in a room. Unlike the conventional VLP models, the proposed model can be used to predict the location even in the presence of multiple objects.
2) Further, we also construct and train a neural network (NN) to estimate the height as well as the radius of the objects. The NN, along with the VLP algorithm, can be together employed to construct a 3-D model of the objects in the room.
3) In addition, we propose a method to optimize the power allocation to each LED in a room by exploiting the current location of objects while maintaining the total power constraint on the system. This will lead to efficient power allocation among LED's, based on the position of objects in the room for optimum communication performance.

The rest of the paper is organized as follows. Section II and III discuss our system model and spatial model respectively. Section IV presents our algorithm for visible light positioning. Section V is related to constructing and training the NN to calculate the height and radius of the objects. Section VI discusses a power allocation scheme for optimum localization accuracy and the paper is concluded in Section VII.

Notations: The vector and the matrix are denoted as $\mathbf{x}$ and $\mathbf{X}$ respectively. The vectorization of matrix $\mathbf{X}$ is denoted as $\mathbf{X}(:)$. The element corresponding to i^{th} row and j^{th} column of a matrix $\mathbf{X}$ is represented as X_{ij}. The blockage probability and the blockage density are denoted as P_B and λ_B, respectively. The actual coordinates of an object is denoted by (x,y) while the predicted coordinated of the object is given by $(\hat{x}, \hat{y})$. The variable L and K are used throughout the paper to denote the number of LED's and the number of objects in the indoor environment. P denotes the power profile of the room and $\mathrm{H}(\tilde{g}, \tilde{l})$ denotes the channel gain between LED (l), and photo diode (g).

II. System Model

In this paper, we have considered a standard office room of dimensions, $5\ \mathrm{m} \times 5\ \mathrm{m} \times 3\ \mathrm{m}$,[2] with 4 LEDs placed on the ceiling. The LEDs are located at the midpoints of the diagonals from the center to the vertices as shown in Fig. 1. The room floor is considered to be the receiver plane and is divided into a number of grids with PDs placed at each grid point.

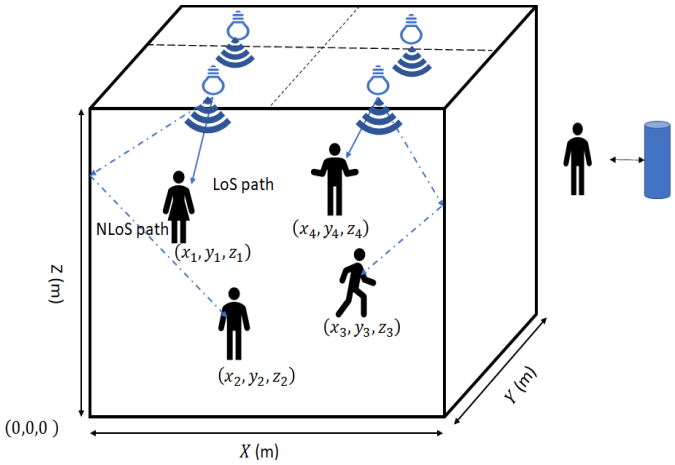

Fig. 1. System model illustrating the location of the LEDs.

The received power at each PD depends on the distance between the LED and the PD, the receiving angle, the field of view of the PD etc. The proposed system model simulates the presence of multiple objects and takes into account a single reflection from the room walls as well as the LoS path. The LoS link is exploited to estimate the position of objects in the indoor environment and their broad geometrical properties like height and radius. The received power profile in the absence of an object can be seen in Fig.2, where each lattice point represents the location of a PD.

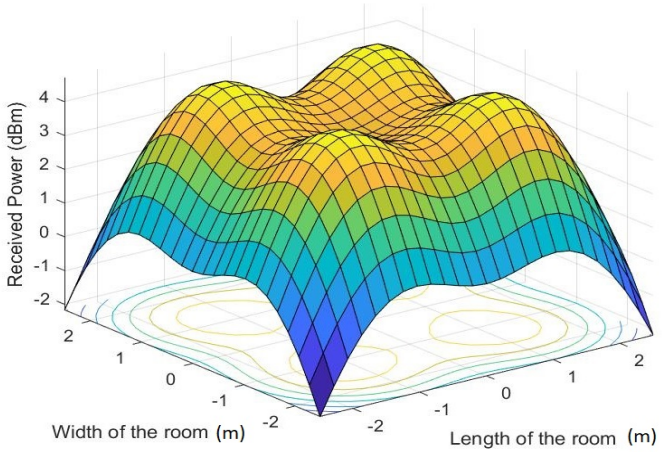

Fig. 2. Received power profile of the room in the absence of any objects.

[2]The dimensions considered are consistent with that of a standard office room as shown in [27].

A. VLC channel Model

We have consider a multipath VLC channel model that includes reflections up to first-order from the wall. In this paper, we have used the integrating-sphere model given in [28]. The integrating-sphere model was originally used in infrared communications, and the most important feature of the model is that the same scattered signal gain is assumed throughout the room.

The frequency response of the channel is given by:

$$H(f) = H(0)\exp(-j2\pi f\Delta\tau_{LoS}) + H_{DIFF}\frac{\exp(-j2\pi f\Delta\tau_{DIFF})}{1+j\left(\frac{f}{f_0}\right)}, \quad (1)$$

where $\Delta\tau_{LOS}$ and $\Delta\tau_{DIFF}$ are the time delays of the transmitted signal taking the LoS and the NLoS path, respectively, f_0 denotes the cut-off frequency of scattering channel, and f represents the operating frequency in Hz.

The channel gain of LoS component, $H(0)$, is given as:

$$H(0) = \begin{cases} \frac{(m+1)A}{2\pi D_d^2}\cos^m(\phi)T_s(\psi)g(\psi)\cos(\psi) \\ 0 \le \psi \le \psi_c \quad , \end{cases} \quad (2)$$

where m represents Lambertian order defined as:

$$m = \frac{-\ln(2)}{\ln(\cos(\phi_{\frac{1}{2}}))} \quad . \quad (3)$$

In (2), A is the physical area of the PD, D_d is the distance between the visible light transmitter and the receiver, ϕ is the angle of irradiance, ψ is the angle of incidence, ψ_c is the receiver field of view (FOV), $T_s(\psi)$ is the gain of the optical filter, and $g(\psi)$ is the gain of the optical concentrator given as:

$$g(\psi) = \begin{cases} \frac{n^2}{\sin^2(\psi_c)}, & 0 \le \psi \le \psi_c, \end{cases} \quad (4)$$

where n is the refractive index of optical concentrator.

The diffuse channel gain H_{DIFF} due to NLoS path is given as:

$$H_{DIFF} = \frac{A_R}{A_{walls}}\frac{\rho}{1-\bar{\rho}} \quad , \quad (5)$$

where,

$$\bar{\rho} = \frac{1}{A_{walls}}\sum_i A_i\rho_i \quad , \quad (6)$$

$\bar{\rho}$ represents an average reflectance, ρ refers to instantaneous reflection, A_R is the area of reflection point on the wall from where the NLoS rays are reflected, A_i is the area of i_{th} grid on the wall and A_{walls} is the total area of the walls of the room over which the reflection is considered.

For a given transmission power (P_T), the total received power using multiple LEDs, including diffused path through the walls, can be obtained as:

$$P_r = \sum_{l=1}^{L}\left[P_T H(0) + \int_{walls} P_T H_{DIFF}\right] \quad . \quad (7)$$

where L is the total number of transmitting LEDs and the total power is obtained by ingratiating both LoS the NLoS links across the room. The parameters used in this paper for the visible light channel are given in Table I.

TABLE I
SYSTEM MODEL PARAMETERS

Parameter	Value
Total transmitted power P_T	2 W
Refractive index n	1.5
Optical filter gain T_s	1
Wall reflection ρ	0.8
LED semiangle Φ	60°
Receiver active area A	1 cm^2
FOV of the receiver ψ_c	60°

III. SPATIAL MODEL

In this paper, the objects are modelled as cylinders placed randomly within the room [29]. Since we have approximated the objects as cylinders, their geometric shape can be determined by their radius and height only. The height of the objects is sampled uniformly from the range 0 to 2 m, and the radius is sampled uniformly from the range 0 to 0.5 m.[3] Unless mentioned otherwise, we will assume the default height and radius of the object to be 1 m and 0.05 m respectively, which are selected keeping in mind the height of the room and the area of the floor.

In this paper, we have used Matern Hard Core Process (MHCP) to generate multiple objects in an indoor environment. Hard-Core processes are point processes where points are not allowed to be closer than a certain minimum distance. Thus, they are more regular (less clustered) than other point processes. Moreover they realistically emulate real-life scenarios where objects have a finite width and cannot occupy the same space. In this paper, we have MHCP Type-I, where we start with a basic uniform Poisson point process (PPP) ϕ_b with intensity λ_b, and then remove all points which have another point within the minimum distance r. The intensity of the type-I process is given by $\lambda_b\, e^{-\lambda_b\pi r^2}$ [30], [31].

IV. PROPOSED VISIBLE LIGHT POSITIONING (VLP) MODEL

In this section, the proposed algorithm for locating an object in an indoor environment is presented. The proposed algorithm takes into account the received power profile of the room in the presence of the objects and estimates the positions of objects in an indoor environment.

A. VLP Model

This subsection discusses the proposed VLP model to estimate the location of the object in a multiple object environment. We have considered an indoor environment having K desired users and L LED light sources. Let P_0 represent the received power profile of the room without any desired users,

[3]These ranges were used keeping in mind the average range for the height and width of humans.

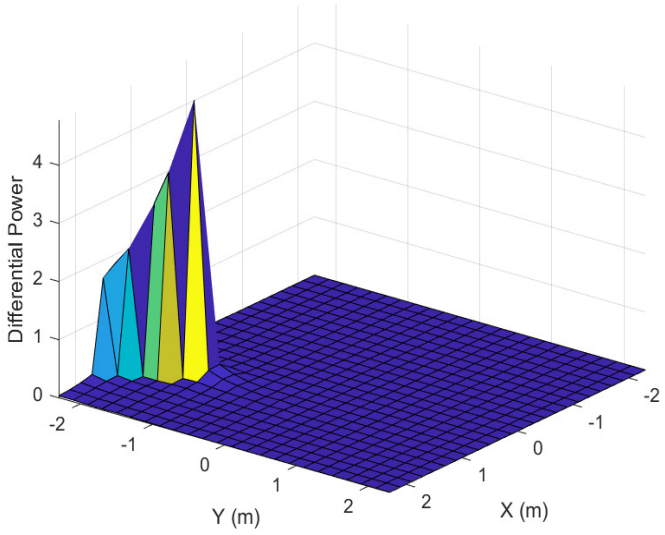

Fig. 3. Differential power profile for an object at (0.6507,-1.2414) with height of 1.4806 which is used to predict the height of the obstacle

and P represent the received power profile in the presence of the desired users. Define a function, $\nabla\mathcal{F} = P_0 - P$, which will be referred as the differential power profile in the rest of the paper. Then the coordinates of the desired users predicted by the system are given such that:

$$(x, y) \ : \nabla\mathcal{F} = 0 \text{ and } \nabla^2\mathcal{F} < 0. \tag{8}$$

Since the function $\nabla\mathcal{F}$ represents the change in the power profile on the addition of desired users in the room, we can assume that the power profile will incur maximum change at points near the location at which the desired users have been added. This assumption has been validated in the results shown in the paper and can be heuristically observed since the desired users block the light reaching the photodiodes in its vicinity and hence have a greater impact on the power profile near their location. For example, Fig. 3 shows the plot of $\nabla\mathcal{F}$, and as you can see, the maxima $(0.65, -1.25)$ lies near the actual location of the obstacle.

However, the power profile cannot be calculated over the entire room, so $\mathcal{F}$ is only evaluated at discrete points known as grid points which contain PDs. The spacing between adjacent grid points is known as grid size (this can be seen in Fig. 1, where each point on the graph is a grid point).

Let $\tilde{g}, \tilde{l}, \tilde{k}$, represent the coordinates of the grid points, LED's and objects respectively.P_0 and P can be evaluated as:

$$(P_0)_{\tilde{g}} = \sum_{l=1}^{L}\left[P_l H_0(\tilde{g},\tilde{l}) + \int_{walls} P_l H_{DIFF}(\tilde{g},\tilde{l})\right], \tag{9}$$

$$P_{\tilde{g}} = \sum_{l=1}^{L}\Bigg[P_l H_0(\tilde{g},\tilde{l})\Big(\prod_{k=1}^{K}\phi(\tilde{g},\tilde{l},\tilde{k})\Big) + \int_{walls} P_l H_{DIFF}(\tilde{g},\tilde{l})\Big(\prod_{k=1}^{K}\phi(\tilde{g},\tilde{l},\tilde{k})\Big)\Bigg]. \tag{10}$$

where, $\phi(\tilde{g},\tilde{l},\tilde{k})$ is an indicator variable (0 or 1), which indicates whether the object is blocking that particular path (0) or not (1), and is calculated geometrically.

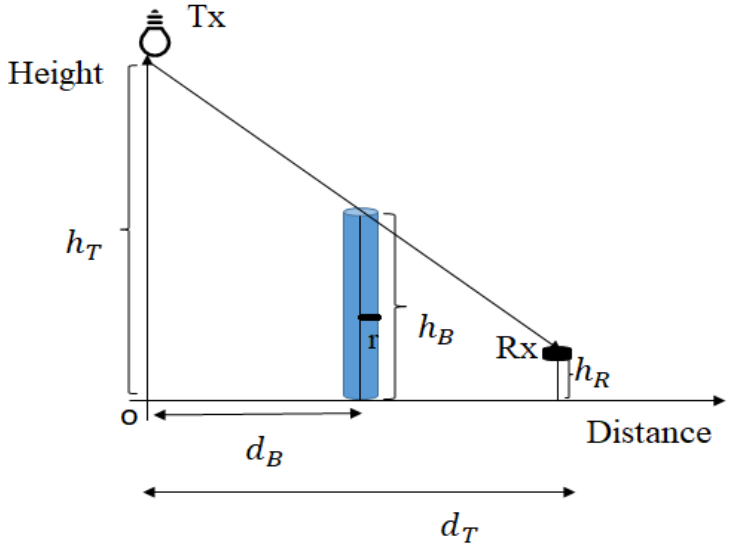

Fig. 4. Schematic for blocking by an object

In the proposed VLC model, an obstacle is said to block the line of sight to the desired user if :

1) The center of the obstacle is at a distance less than r from the line joining the center of the desired user to the LED, where r is the radius of the obstacle (Please ref. Fig. 4).
2) The height of obstacle is sufficient such that its shadow reaches the desired user, which can also be checked geometrically. As shown in Fig. 4, the condition is equivalent to:

$$\frac{h_B - h_R}{d_B} \geq \frac{h_T - h_R}{d_T}$$

where h_B is the height of the obstacle, h_R is the height of the receiver, h_T is the height of LED, and d_T and d_B are the horizontal distances of user and blockages from the transmitting LED respectively.

B. Performance of VLP algorithm

In this subsection, the performance of the proposed VLP algorithm has been presented. In order to test the performance, an object is uniformly simulated inside the room with the default shape (height and width) parameters. The location of this object is then estimated using the VLP algorithm, and this process is repeated over 1000 iterations.

The average root mean square error (RMSE) thus obtained in the measurement is **0.054 m**, where the RMSE is calculated as:

$$\text{RMSE} = \sqrt{\sum_{n=1}^{N} \frac{(\hat{x}-x)^2 + (\hat{y}-y)^2}{N}}. \tag{11}$$

where $\hat{x}, \hat{y}$ represents the predicted location of the desired user and x, y represent the true location of the desired user, and N is the total number of iterations which in the present case is equal to 1000.

C. Variation of VLP system performance with system parameters

The proposed algorithm can also be applied to a multiple object environment. However, the interference with the line of sight and shadowing effects in a multiple object scenario would result in lower location accuracy. In this subsection, the impact of grid size and the number of objects on the performance of the proposed VLP algorithm is discussed.

1) Grid Size

In the practical system, the power profile of the room can only be evaluated at discrete points across the room. The grid size (the distance between two adjacent points at which the function is evaluated) is extremely important for two reasons. Firstly, it decides the number of PDs required for the system to function. Larger the grid size, lesser the number of PDs required. However for a smaller grid size the function is evaluated at more number of points, and it approximates the continuous function better. Hence, the error in VLP is expected to increase with grid size.

The effect of varying the grid size on the RMSE, average location error over multiple iterations can be seen in Fig. 5. For each value of grid size, 20 iterations of multiple desired user environments are generated using MHCP, and for each iteration, the location error (ϵ) is calculated as:

$$\epsilon = \sum_{k=1}^{K} \frac{\sqrt{(\hat{x}-x)^2 + (\hat{y}-y)^2}}{K}. \tag{12}$$

where, $\hat{x}, \hat{y}$ represent the predicted location of the desired user and x, y represent the true location of desired user, and K represents the number of desired users generated using MHCP in that particular iteration.

Fig. 5 shows the variation in location error with varying grid sizes. It can be seen that the location error increases with the increase in grid size which is consistent with our hypothesis considered in the paper. It is due to the fact that the smaller the grid size, the better the approximation to the continuous differential power profile and hence our algorithm works better too. Unless otherwise mentioned in this paper, henceforth, we will assume a grid size of 0.2 m as a further decrease in grid size increase the operational overload without any proportionate increase in accuracy of the model as seen in Fig. 5.

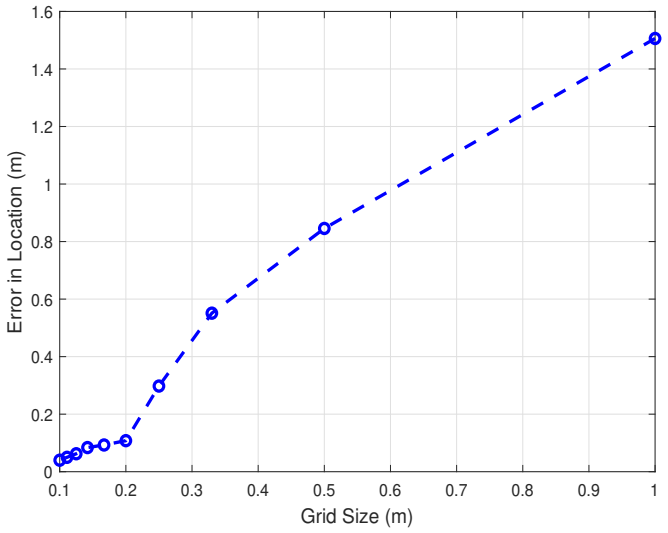

Fig. 5. Variation of location error with grid size

2) Number of objects

Since the MHCP results in a random number of objects being generated in the room, in order to get a fixed number of objects, we will be using a random point process which assumes a uniform probability of an object being anywhere in the room. Moreover, the objects are distributed independently with the same default shape parameters (height, radius).

Fig. 6 depicts the variation of location error with a change in the number of objects. The location error is calculated using (12).

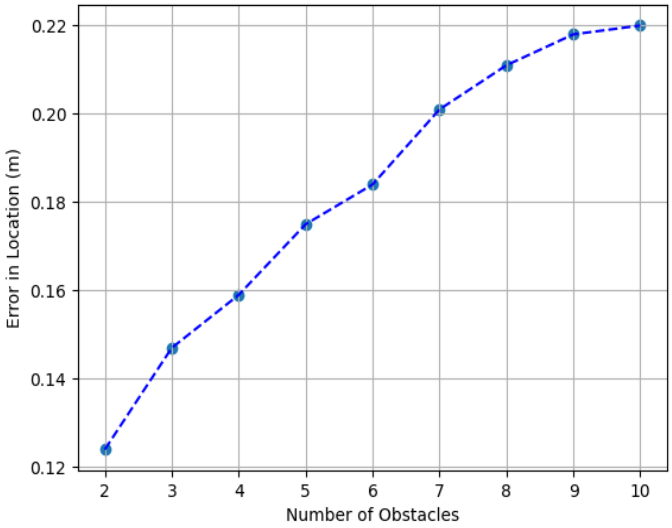

Fig. 6. Variation of location error with the number of obstacles

As we can see, the value of location error increases with the number of objects. More the number of objects in a room, greater will be the probability of an object being blocked by another's shadow. This overlap would result in some objects

not being detected which increases the error in positioning as shown in Fig. 6.

V. Shape Estimation using Visible Light

This section presents a novel insight into using visible light to construct a 3-D rendering of an indoor environment. This algorithm can be used to develop accurate surveillance systems which makes use of only the current lighting infrastructure of the rooms. Moreover, using LED's is much cheaper than the present methods of height estimation that utilizes microwave or WiFi. Estimating the shape of objects in an indoor environment could help us in constructing a topological map of the room which could be useful for indoor navigation and monitoring.

One of the most significant advantages of the system model presented in this paper over the previous system models is its ability to estimate an object/ user's shape in the room's boundaries. Since we are modelling the objects as cylinders, estimating their shape consists of estimating the height and radius of the objects. No extra hardware is required for shape estimation, and instead, it can be done using the same architecture, LEDs as transmitters and PDs as the receiver. However, it can not be done using a fixed algorithm since height and radius estimation are more subjective than location estimation. In this paper, we have constructed a NN as shown in Fig. 7, that takes the room's received power profile as input and then outputs the predicted height/radius of the object [32]–[36].

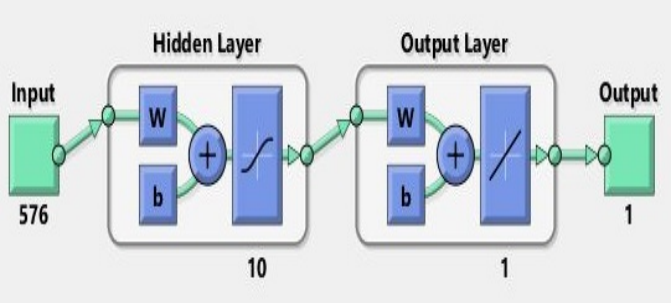

Fig. 7. Structure of the shallow neural network [37], [38] used for shape estimation

A. Height Estimation Model

The height of an object in a room is calculated by constructing an artificial NN. It takes the received power profile of the room as an input and predicts the height of the object. The received power profile of the room consists of power received at each grid point in the room. The height of the objects is assumed to be between 0 and 2 m, which is a reasonable range for indoor measurements. The radius of the object is fixed at the default value of 0.05 m.

1) Training Data generation

In order to make predictions using a NN, the first step is to train the parameters of the NN in order to minimize the error in predicting the height of objects. We simulate an object at a random location in the room with uniform probability across the entire room and sample the object's height from a uniform distribution between 0 to 2 m. Further, we calculate the differential power profile of the room in the presence of the object. This is repeated over 1000 iterations to get a training dataset. It is seen that the NN works better when the target variable is between [0,1], so the height of the sample is divided by 2 and used to train the network. The height predicted by the NN is then doubled in order to get the actual predicted height. Where, X and Y represent the length and the width of the room respectively.

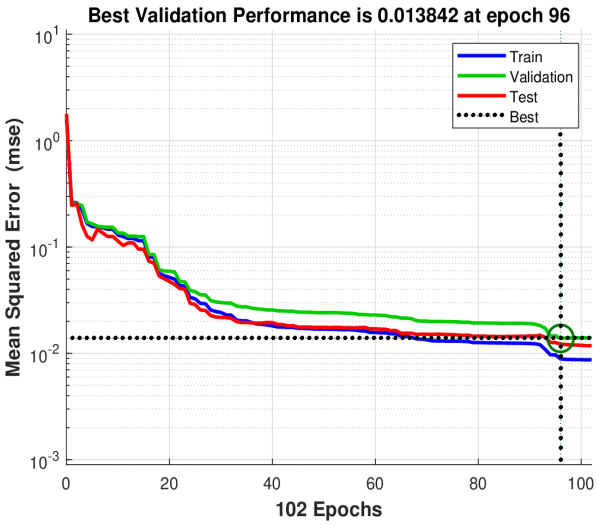

Fig. 8. Training the neural network

2) Training NN

For training, the constructed data set is divided in the proportion of 80:10:10 into the training, validation, and test set. A shallow NN having 10 hidden nodes is constructed and then trained using the Levenburg-Marquadt (LM) algorithm.

The LM algorithm iteratively finds the minima of a function that can be expressed as the sum of squares of non-linear functions. It is very useful in solving problems involving non-linear least squares and is a combination of the Gauss-Newton method and Steepest Gradient Descent [39].

3) Results

The NN was trained for over 100 epochs (Please ref. Fig. 8) after which the error obtained in each of the training, validation and testing sets is represented below in Table II. The best performance of the NN is seen at epoch 102, that is minimum RMSE was seen in the test set.

TABLE II
Distributed Error in Prediction

Data type	Samples	RMSE	R-value
Training	800	4.38854e-2	9.421e-1
Validation	100	6.08677e-2	9.1654e-1
Testing	100	5.60280e-2	9.0426e-1

RMSE is defined as the average squared difference between

the outputs of the NN and targets, which are the true values. Lower values of RMSE means a more accurate prediction by the NN. Regression (R) values is indicative of the correlation between targets and outputs [40]. An R value close to 1 means that the output and the target are strongly co related that is there exists a simple bijective mapping between the two. On the other hand, an R value of 0 indicates a random relationship. The performance of the NN is better represented by Figs. 9 and 10.

Fig. 9 depicts the distribution of errors over the training, validation and test set. It is an histogram with the height of the bar equal to the number of instances with error equal to the range on the x axis. As you can see that the error distribution is sharply peaked around zero error and the number of instances become close to zero as the amount of error increases. This shows that the neural network model is working correctly and predicting values close to the intended target. Fig. 10 shows us the regression value for the training, validation and test set as well as over the entire dataset. As you can see that we get an almost direct correlation between the outputs predicted by the neural network and the target variables. This shows that the model is working correctly in predicting the target variable.

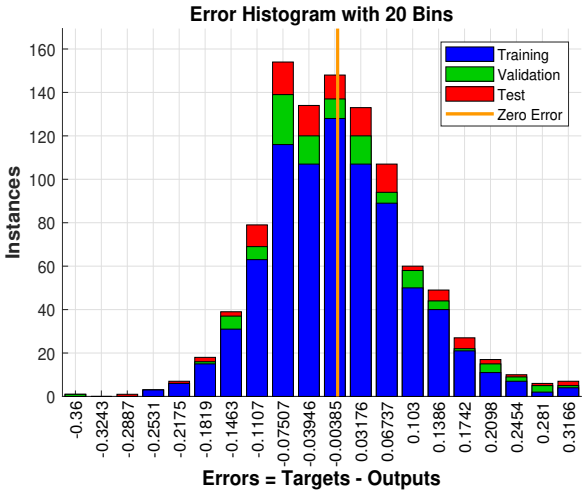

Fig. 9. Distribution of error in prediction by the NN

B. Radius Estimation Model

The radius of an object in a room is calculated by constructing an artificial NN. That takes the power profile of the room as an input and predicts the radius of the object. The power profile of the room consists of power received at each grid point in a room that contains a PD. The radius of the objects is taken between 0 and 0.5 m, which is a reasonable range for indoor measurements. The height of the object is fixed at the default value of 1 m.

1) Creating Training Data

In order to make predictions using a NN, the first step is to train the parameters of the NN in order to minimize the error in predicting the height of objects. An object is repeatedly

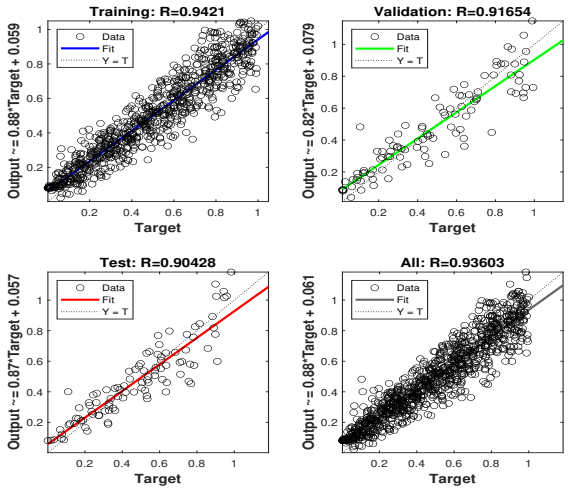

Fig. 10. R values for the data in each of the training, validation and test set as well as the entire dataset

simulated for 1000 iterations at a random location in the room with uniform probability over the entire room. The object radius is sampled from a uniform distribution between 0 to 0.5 m. The power profile of the room is then taken as input to the NN to calculate the object radius. It is seen that the NN works better when the target variable is between [0,1], so the height of the sample is doubled and used to train the network. The radius calculated by the NN is then halved to get the actual predicted radius.

2) Training NN

For training, the constructed data set is divided in the proportion of 80:10:10 into the training, validation, and test set. A shallow NN with 10 hidden nodes is then constructed and trained using the Bayesian regularization algorithm as shown in Fig. 11.

Bayesian regularization is a commonly used process to train Neural networks and is especially used to convert non linear regression into a simple ridge regression. It offers many advantages such as: the models are more robust, the validation process is faster and models become difficult to overtrain and overfit [41].

3) Results

The NN was trained for over 100 epochs after which the error obtained in each of the training, validation and testing sets is represented in Table III. The best performance of the NN was seen at epoch 104, that is the minimum RMSE was seen in the test set.

TABLE III
ERROR IN PREDICTION

Data type	Samples	RMSE	R-value
Training	800	1.26084e-2	9.027e-1
Validation	100	1.14627e-2	8.5783e-2
Testing	100	1.47891e-2	8.757e-1

Lower values of RMSE means a more accurate prediction by the NN. Regression (R) values is indicative of the correlation

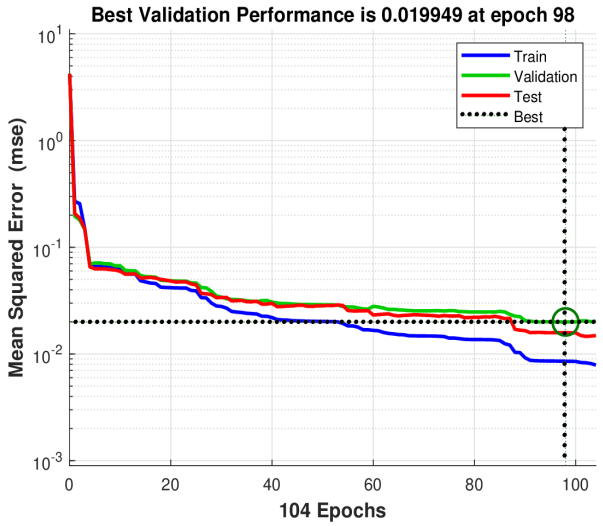

Fig. 11. Training the neural network

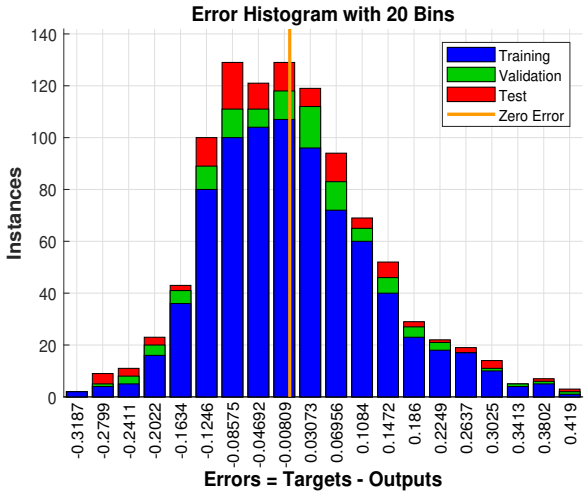

Fig. 12. Distribution of error in prediction by the NN

between targets and outputs [40]. An R value close to 1 means that the output and the target are strongly co related that is there exists a simple objective mapping between the two. On the other hand, an R value of 0 indicates a random relationship. The performance of the NN is better represented in Figs. 12 and 13.

Similar observations can be seen in Fig. 12 and 13 to height estimation. The error for radius estimation is also sharply peaked around zero error and becomes no of instances become rarer as the amount of error increases. The regression values shown in Fig. 13 are also very close to 1 showing a direct correlation between the outputs of the neural network and the target variable. Based on the above two points, we can safely say that our radius estimation model is working correctly and is predicting values close to the target variable. One observation that we can draw from the Fig. 12 is that the network tends to underestimate the radius more often which may be due to the shadowing effects of other objects.

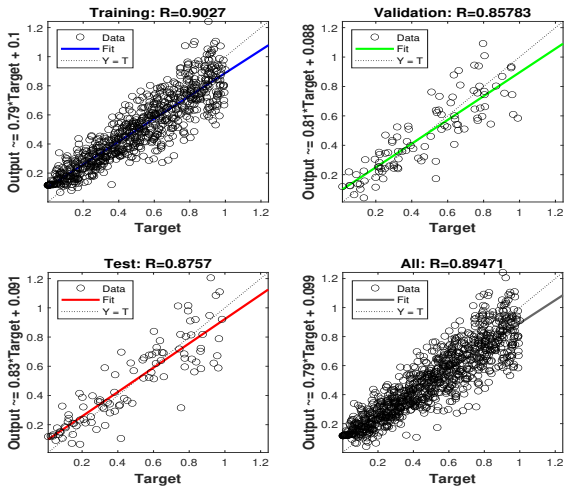

Fig. 13. R values for the data in each of the training, validation and test set as well as the entire data set

VI. Optimising VLP by changing Power Allocation to LED's

In this section, we have analyzed the performance of the proposed VLP system by optimizing the power allocation to LEDs. The proposed optimal LED power allocation framework is based on human blockage estimation inside the room. The objective is to maximize the power at the receiver (user end) subject to the illumination and BER constraints. Here, we consider multiple LEDs and multiple user scenarios wherein each user will act as a human blockage to others. Further, in order to update the LED power with respect to the user's location inside the room, we require an estimation of the user location, which is further fed into the LED controller, which distributes the power among LEDs as per the proposed optimal LED power allocation. Here we can deploy a microcontroller-based LED controller circuit to facilitate the power management (varying light intensity) of the LEDs based on the user's location information inside the room.

In the system model, we have first simulated using an infinitely thin obstacle and then using an obstacle having a radius of 0.05m. Linear Regression is applied to the results to develop a predictive algorithm to obtain the location and height of an obstacle from the received power profile. Initially, when no information about the location of the user (also the obstacle for the other users) is available, power is allocated equally to all the LED's. Once the location information is available, initially, total power is allocated to one particular LED at a time while leaving the other 3 LEDs with no power, and the location error is calculated. Then the process is repeated for all the LEDs until the location information of each user is obtained. Afterward, power is allocated in such a way that the

LED serving the more users will get the more power giving the minimum location error with respect to other LEDs having fewer users, respectively.

Let us consider the power allocated to the LED in the form of a four-dimensional vector, P, where each entry represents the power allocated to that LED.

$$P = \begin{bmatrix} P_1 \\ P_2 \\ P_3 \\ P_4 \end{bmatrix}, \tag{13}$$

where, P_i is the power allocated to the i^{th} LED , $i = \{1, 2, 3, 4\}$, subject to the total power constraint:

$$\sum_i P_i = P_t, \tag{14}$$

where P_t is the total power. The proposed power allocation algorithm is given by:

Algorithm 1: Power Allocation Algorithm

Result: Optimum power allocation vector, $\mathbf{\Phi}$

Initial power allocation vector, P

$P_i = \frac{P_t}{4} \ \ \forall i = \{1, 2, 3, 4\}$

For j = {1,2,3,4}

- Set Power allocation vector, $\mathbf{P^j}$, such that $P_i^j = P_t\ \delta_{ij}$
- Simulate the received power profile of the room and then calculate $\mathrm{Location\_Error}_j$ using Section IV

Set,

$$\Phi_i = \frac{\frac{1}{\mathrm{Location\_Error}_i}}{\sum_{j=1}^{4} \frac{1}{\mathrm{Location\_Error}_j}}.$$

where, δ_{ij} is the dirac delta function.

$$\delta_{ij} = \begin{cases} 0 & i \neq j \\ 1 & i = j \end{cases} \tag{15}$$

Here, Eq. (15) defines the Kronecker delta function, δ_{ij} which is equal to unity only when $i = j$ and is zero for all other values of i and j. Where index i and j are for the LED and the user, respectively. So the power allocation is done only when there is a link available between i_{th} LED and the j_{th} user.

The performance of this system model can be seen for particular arrangements of objects as shown in the Fig. 14. From the snapshot, it can be observed that instead of allocating more power to the LED around which some objects are clustered, our allocation scheme allocates more power to the LED from which the average distance of all the objects is lesser. This power allocation algorithm was applied over many iterations, where each iteration has a different number and arrangement of obstacles, to improve positioning by optimizing the power allocation to LED's.

Over 100 iterations, the power allocation optimization was applied, and the algorithm showed improvements in location accuracy in 20 iterations, with the accuracy remaining unchanged in the rest. We can conclude that there is a saturation point for the accuracy after which application of the algorithm

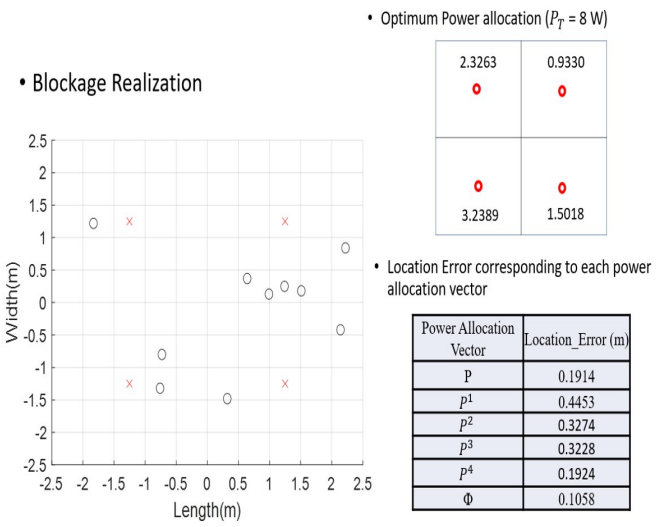

Power Allocation Vector	Location_Error (m)
P	0.1914
P^1	0.4453
P^2	0.3274
P^3	0.3228
P^4	0.1924
Φ	0.1058

Fig. 14. Position of objects, power allocated to the LED's and the location error

provides no further improvement. The saturation point varies widely for different arrangements of the objects in the room and it is difficult to quantify it. The optimization algorithm resulted in an average net improvement of 22.068 % (9.2 cm) in location accuracy.

VII. Conclusion

This paper introduces a novel VLP model which can be used to predict the location of an object even in multiple object environments. It is seen that the minimum squared error for positioning is 6.7 cm. Moreover, the effect of grid size (the distance between two adjacent PDs) and the number of objects on the location error is also observed. In addition, this paper also presents a NN-based algorithm for measuring the height and radius of objects in an indoor environment such that a 3-D rendering of the room can be constructed. The RMSE for the height and radius of the objects is 4.67 cm and 1.27 cm, respectively. Moreover, the regression values obtained for both height and radius show a clear dependence between the output of the NN and the target value.

Furthermore, in this paper, we have discussed a method for optimizing the power allocation to the LEDs in the room, such that optimum location accuracy can be obtained, keeping the total power of LEDs constant. The algorithm proposed shows an improvement in 20% of the cases, with an average improvement of 9.2 cm. An important point to be noted is that on the application of the algorithm, the error in positioning either decreases or remains the same, it never increases. In addition to the results presented above, this paper opens up the doors to many exciting research prospects like using the above methods to jointly estimate the radius and height of the obstacles. The proposed algorithm could find applications in remote surveillance and monitoring of indoor environments using just LEDs and PDs.

REFERENCES

[1] M. E. Rida, F. Liu, Y. Jadi, A. A. A. Algawhari, and A. Askourih, "Indoor location position based on bluetooth signal strength," in *2015 2nd International Conference on Information Science and Control Engineering*. IEEE, 2015, pp. 769–773.

[2] C. Yang and H.-R. Shao, "WiFi-based indoor positioning," *IEEE Communications Magazine*, vol. 53, no. 3, pp. 150–157, 2015.

[3] X.-Y. Lin, T.-W. Ho, C.-C. Fang, Z.-S. Yen, B.-J. Yang, and F. Lai, "A mobile indoor positioning system based on ibeacon technology," in *2015 37th Annual International Conference of the IEEE Engineering in Medicine and Biology Society (EMBC)*. IEEE, 2015, pp. 4970–4973.

[4] R. Harle, "A survey of indoor inertial positioning systems for pedestrians," *IEEE Communications Surveys & Tutorials*, vol. 15, no. 3, pp. 1281–1293, 2013.

[5] C.-H. Huang, L.-H. Lee, C. C. Ho, L.-L. Wu, and Z.-H. Lai, "Real-time RFID indoor positioning system based on kalman-filter drift removal and heron-bilateration location estimation," *IEEE Transactions on Instrumentation and Measurement*, vol. 64, no. 3, pp. 728–739, 2014.

[6] N. U. Hassan, A. Naeem, M. A. Pasha, T. Jadoon, and C. Yuen, "Indoor positioning using visible LED lights: A survey," *ACM Computing Surveys (CSUR)*, vol. 48, no. 2, pp. 1–32, 2015.

[7] X. Zhang, J. Duan, Y. Fu, and A. Shi, "Theoretical accuracy analysis of indoor visible light communication positioning system based on received signal strength indicator," *Journal of Lightwave Technology*, vol. 32, no. 21, pp. 3578–3584, 2014.

[8] P. Huynh and M. Yoo, "VLC-based positioning system for an indoor environment using an image sensor and an accelerometer sensor," *Sensors*, vol. 16, no. 6, p. 783, 2016.

[9] L. Li, P. Hu, C. Peng, G. Shen, and F. Zhao, "Epsilon: A visible light based positioning system," in *11th USENIX Symposium on Networked Systems Design and Implementation (NSDI 14)*, 2014, pp. 331–343.

[10] S.-Y. Jung and C.-S. Park, "Lighting LEDs based indoor positioning system using received signal strength ratio," *Proceedings of 3DSA2013*, vol. 8, no. 5, 2013.

[11] A. Singh, A. Srivastava, V. A. Bohara, and A. K. Jagadeesan, "Performance of indoor VLC system under random placement of LEDs with nonimaging and imaging receiver," *IEEE Systems Journal*, pp. 1–12, 2020.

[12] Y. Gu, A. Lo, and I. Niemegeers, "A survey of indoor positioning systems for wireless personal networks," *IEEE Communications Surveys & Tutorials*, vol. 11, no. 1, pp. 13–32, 2009.

[13] M. Jacob, S. Priebe, T. Kürner, M. Peter, M. Wisotzki, R. Felbecker, and W. Keusgen, "Fundamental analysis of 60 GHz human blockage," in *2013 7th European Conference on Antennas and Propagation (EuCAP)*, 2013, pp. 117–121.

[14] M. Gapeyenko, A. Samuylov, M. Gerasimenko, D. Moltchanov, S. Singh, E. Aryafar, S.-p. Yeh, N. Himayat, S. Andreev, and Y. Koucheryavy, "Analysis of human-body blockage in urban millimeter-wave cellular communications," in *2016 IEEE International Conference on Communications (ICC)*, 2016, pp. 1–7.

[15] A. Chakraborty, A. Singh, V. A. Bohara, and A. Srivastava, "A visible light communication based predictive system for the height and location estimation of an obstacle," in *2020 IEEE International Conference on Advanced Networks and Telecommunications Systems (ANTS)*, 2020, pp. 1–6.

[16] S. Shawky, M. A. El-Shimy, Z. A. El-Sahn, M. R. M. Rizk, and M. H. Aly, "Improved VLC-based indoor positioning system using a regression approach with conventional RSS techniques," in *2017 13th International Wireless Communications and Mobile Computing Conference (IWCMC)*, 2017, pp. 904–909.

[17] A. Şahin, Y. S. Eroğlu, I. Güvenç, N. Pala, and M. Yüksel, "Hybrid 3-D localization for visible light communication systems," *Journal of Lightwave Technology*, vol. 33, no. 22, pp. 4589–4599, 2015.

[18] S. Bastiaens, W. Raes, N. Stevens, L. Martens, W. Joseph, and D. Plets, "Impact of a photodiode's angular characteristics on RSS-based VLP accuracy," *IEEE Access*, vol. 8, pp. 83 116–83 130, 2020.

[19] X. Yu, J. Wang, and H. Lu, "Single LED-based indoor positioning system using multiple photodetectors," *IEEE Photonics Journal*, vol. 10, no. 6, pp. 1–8, 2018.

[20] G. Simon, G. Zachár, and G. Vakulya, "Lookup: Robust and accurate indoor localization using visible light communication," *IEEE Transactions on Instrumentation and Measurement*, vol. 66, no. 9, pp. 2337–2348, 2017.

[21] R. Amsters, D. Holm, J. Joly, E. Demeester, N. Stevens, and P. Slaets, "Visible light positioning using bayesian filters," *Journal of Lightwave Technology*, vol. 38, no. 21, pp. 5925–5936, 2020.

[22] H. Cheng, C. Xiao, Y. Ji, J. Ni, and T. Wang, "A single LED visible light positioning system based on geometric features and CMOS camera," *IEEE Photonics Technology Letters*, vol. 32, no. 17, pp. 1097–1100, 2020.

[23] B. Zhou, V. Lau, Q. Chen, and Y. Cao, "Simultaneous positioning and orientating for visible light communications: Algorithm design and performance analysis," *IEEE Transactions on Vehicular Technology*, vol. 67, no. 12, pp. 11 790–11 804, 2018.

[24] Y. Cai, W. Guan, Y. Wu, C. Xie, Y. Chen, and L. Fang, "Indoor high precision three-dimensional positioning system based on visible light communication using particle swarm optimization," *IEEE Photonics Journal*, vol. 9, no. 6, pp. 1–20, 2017.

[25] A.-C. Anastou, K. K. Delibasis, A.-A. A. Boulogeorgos, H. G. Sandalidis, A. Vavoulas, and S. K. Tasoulis, "A low complexity indoor visible light positioning method," *IEEE Access*, vol. 9, pp. 57 658–57 673, 2021.

[26] J. Xu, H. Shen, W. Xu, H. Zhang, and X. You, "LED-assisted three-dimensional indoor positioning for multiphotodiode device interfered by multipath reflections," in *2017 IEEE 85th Vehicular Technology Conference (VTC Spring)*, 2017, pp. 1–6.

[27] P. Chvojka, S. Zvanovec, P. A. Haigh, and Z. Ghassemlooy, "Channel characteristics of visible light communications within dynamic indoor environment," *Journal of Lightwave Technology*, vol. 33, no. 9, pp. 1719–1725, 2015.

[28] V. Pohl, V. Jungnickel, and C. Von Helmolt, "Integrating-sphere diffuser for wireless infrared communication," *IEE Proceedings-Optoelectronics*, vol. 147, no. 4, pp. 281–285, 2000.

[29] A. Singh, G. Ghatak, A. Srivastava, V. A. Bohara, and A. K. Jagadeesan, "Performance analysis of indoor communication system using off-the-shelf LEDs with human blockages," *IEEE Open Journal of the Communications Society*, vol. 2, pp. 187–198, 2021.

[30] B. Matérn, *Spatial variation*. Springer Science & Business Media, 2013, vol. 36.

[31] J. Teichmann, F. Ballani, and K. G. van den Boogaart, "Generalizations of matérn's hard-core point processes," *Spatial Statistics*, vol. 3, pp. 33–53, 2013.

[32] R. Rojas, "The backpropagation algorithm," in *Neural networks*. Springer, 1996, pp. 149–182.

[33] J. Li, J.-h. Cheng, J.-y. Shi, and F. Huang, "Brief introduction of back propagation (BP) neural network algorithm and its improvement," in *Advances in Computer Science and Information Engineering*. Springer, 2012, pp. 553–558.

[34] Y. Li and Y. Yuan, "Convergence analysis of two-layer neural networks with relu activation," *arXiv preprint arXiv:1705.09886*, 2017.

[35] X. Yu, M. O. Efe, and O. Kaynak, "A general backpropagation algorithm for feedforward neural networks learning," *IEEE Transactions on Neural Networks*, vol. 13, no. 1, pp. 251–254, 2002.

[36] J. Jantzen, "Introduction to perceptron networks," *Technical University of Denmark, Lyngby, Denmark, Technical Report*, 1998.

[37] W. S. McCulloch and W. Pitts, "A logical calculus of the ideas immanent in nervous activity," *The Bulletin of Mathematical Biophysics*, vol. 5, no. 4, pp. 115–133, 1943.

[38] J. E. Dayhoff, *Neural network architectures: an introduction*. Van Nostrand Reinhold Co., 1990.

[39] A. Ranganathan, "The levenberg-marquardt algorithm," *Tutoral on LM Algorithm*, vol. 11, no. 1, pp. 101–110, 2004.

[40] C. Cheng, K. Chau, Y. Sun, and J. Lin, "Long-term prediction of discharges in manwan reservoir using artificial neural network models," in *International Symposium on Neural Networks*. Springer, 2005, pp. 1040–1045.

[41] F. Burden and D. Winkler, "Bayesian regularization of neural networks," *Artificial Neural Networks*, pp. 23–42, 2008.